Progress In Electromagnetics Research C, Vol. 129, 115–126, 2023

Design and Experimental Verification of Variable Flux Permanent Magnet Vernier Machine Using Time-Stepping Finite Element Method

Yang Zhang[1, 2], Jiming Luo[1, *], Mingming Huang[1, 2], Quanzhen Huang[1, 2], and Duane Decker[3]

Abstract—A novel variable flux permanent magnet vernier machine (VFPMVM) is proposed by introducing the concept of hybrid excitation, and its flux modulation poles (FMPs) and excitation winding are emplaced in stator teeth and the adjacent FMPs, respectively. It can offer several merits, such as wide speed range operation through the processing of flux-enhancing and flux-weakening without increasing machine bulk, as well as the numbers of stator slot and rotor pole. Moreover, as one sort of flux modulation machine based on magnetic field modulation effect, VFPMVM features low speed, large torque, simpler mechanical structure and better utilization of PM materials than traditional flux modulation machines. The working principle of proposed machine is studied, and basic electromagnetic characteristics are calculated by finite element method, including no-load magnetic flux linkage, no-load back electromotive force, cogging torque, and output torque. In addition, the processes of flux-enhancing and flux-weakening are analyzed. Finally, one prototype with one kilowatt was built, and its static characteristics were tested. The results show that the proposed VFPMVM has the merits of high torque density, small cogging torque, and wide speed range, which is a promising candidate for electric vehicle direct drive field.

1. INTRODUCTION

Permanent magnet synchronous machine (PMSM) features obvious merits in power density and efficiency due to the improvement of high-performance permanent magnet (PM) material manufacturing technology in past decades, and its application has been increased rapidly in different industrial fields [1, 2]. For low-speed direct drive industrial applications, such as electric vehicles (EVs), direct drive PMSM owns gearless transmission, which can avoid a series of problems caused by mechanical gear transmission, such as mechanical friction and low transmission efficiency [3]. Hence, low speed direct drive PMSM is one promising option for the applications of direct drive industry, which has become a research hotspot because of its high efficiency, long service life, and strong reliability [4]. However, with the purpose of achieving low speed and high torque, the number of pole slots of traditional direct drive PMSM is generally large, which leads to large machine volume and brings great difficulties to manufacturing, assembly, and transportation [5].

With the introduction and application of non-contact magnetic gear, high torque density magnetic field modulation machine based on magnetic gear effect has come into one feasible solution in recent years. By combining concentric magnetic field modulated magnetic gear with traditional PMSM, magnetic gear composite permanent magnet machines are proposed in [6], respectively. This kind of

Received 21 November 2022, Accepted 16 January 2023, Scheduled 29 January 2023

* Corresponding author: Jiming Luo (hngcxy_ljm@163.com).

[1] School of Electrical Information Engineering, Henan University of Engineering, Zhengzhou 451191, China. [2] Power Integration and Intelligent Control Center, Industrial Software Industry Research Institute, Henan University of Engineering, Zhengzhou 451191, China. [3] School of FOCUS Engineering, Portland State University, Portland, P. O. Box 751, USA.

machine combines the advantages of outer rotor PMSM and novel magnetic gear, and greatly improves the output torque under the same parameters. Many research achievements about magnetic gears, magnetic gear machine, and magnetic field modulation machines were obtained by Chau's group, such as magnetic-geared outer-rotor permanent-magnetic brushless motor [7], coaxial magnetic gear analytical approach [8], electronic-continuously variable transmission system for hybrid electric vehicles (HEVs) [9], magnetic-gear-integrated wind power generator [10], coaxial magnetic gear modulating effect optimization [11], quantitative comparisons of flux-modulated interior permanent magnet machines with distributed dindings and concentrated windings [12], permanent magnet flux modulated machine and vernier machine for wind power generation [13, 14]. However, the theoretical magnetic field analysis and manufacturing of this sort of compound machine are relatively complex due to a three-layer air gap structure, which limits its industrial application. Based on prior studies above mentioned, various types of novel magnetic field modulation machines (MFMMs) have been designed and developed in [15–19]. Compared with the magnetic gear composite machines, MFMMs have simple structures and convenient processing. Compared with the magnetic gear composite motor, this type of motor has a simple structure and convenient manufacturing. The single-layer air gap structure enables it to fully use the analysis, design, and computering methods of conventional PMSM. It should be noticed that the torque density of MFMMs has been greatly improved compared with the traditional PMSMs, which is verified by experimental prototypes. The magnetic concentrating single tooth open slot MFMM is proposed in [20], whose topology appearance resembles the case in [6] except the embedded PM structure. Its stator teeth act as a magnetic flux modulation pole, and the number of stator slots is not reduced compared with traditional PMSM. The concept of memory machine was introduced into vernier machine, and a novel kind of memory PM vernier machines for electric vehicle was proposed in literatures [21]. The concept of flux modulation pole (FMP) was introduced into the stator tooth topology of magnetic gear machine, and a multi-tooth split pole external rotor MFMM was proposed in [22], which can effectively reduce machine loss with adopting concentrated winding. FMP acts as a magnetic regulating ring in the magnetic gear machine, which plays the role of modulating the air-gap magnetic conductance. In addition, a flux-controllable vernier permanent-magnet machine was also proposed by Chau's team in [23], by artfully integrating the vernier structure and the DC field winding together, respectively, to fulfil the purpose of controllable magnetic flux and increase the machine operation range. However, it should be noticed that the simultaneous arrangement of armature winding and DC excitation winding in the limited stator space could cause the low utilization of stator space and large temperature rise. From the perspectives of machine topology and operation principle, it can be concluded that the above mentioned vernier machines belong to the MFMM.

This paper is organized as follows. Section 1 presents the proposed VFMFMM topology and design methodology. Section 2 gives the proposed machine's operation principle and torque expression. Electromagnetic characteristics of the machine, such as no-load PM flux linkage, induced electromotive force, cogging torque, and output torque, are calculated and analyzed using finite element method in Section 3. Several experimental verifications and conclusion are presented in Section 4 and Section 5, and the performance changes of the machine with and without DC excitation are calculated and compared, respectively.

2. TOPOLOGY OF VFMFMM

In order to achieve variable flux as well as magnetic flux modulation effect, a VFMFMM is engaged, whose configuration is shown in Fig. 1(a) and Fig. 1(b). Different from the existing MFMM, there are nine slots in the inner stator, which are occupied by three-phase concentrated armature windings. Moreover, the DC excitation windings are evenly distributed between adjacent FPMs. Each stator tooth is split into two flux modulation poles (FMPs), thus constituting 18 FMPs in total, which function to modulate the low-speed rotating PM field of the outer rotor to high speed rotating field in stator. Fourteen pole-pairs of PMs are embedded in the outer rotor along the circumferential direction, which feature the machine with obvious flux concentrating effect. The machine stator armature winding connection and its star slot diagram are shown in Fig. 2.

It can be seen from Fig. 1 and Fig. 2 that topology of the proposed VFPMVM features the following advantages: (1) The proposed VFMFMM originates from the traditional PMVM, hence, it inherits the

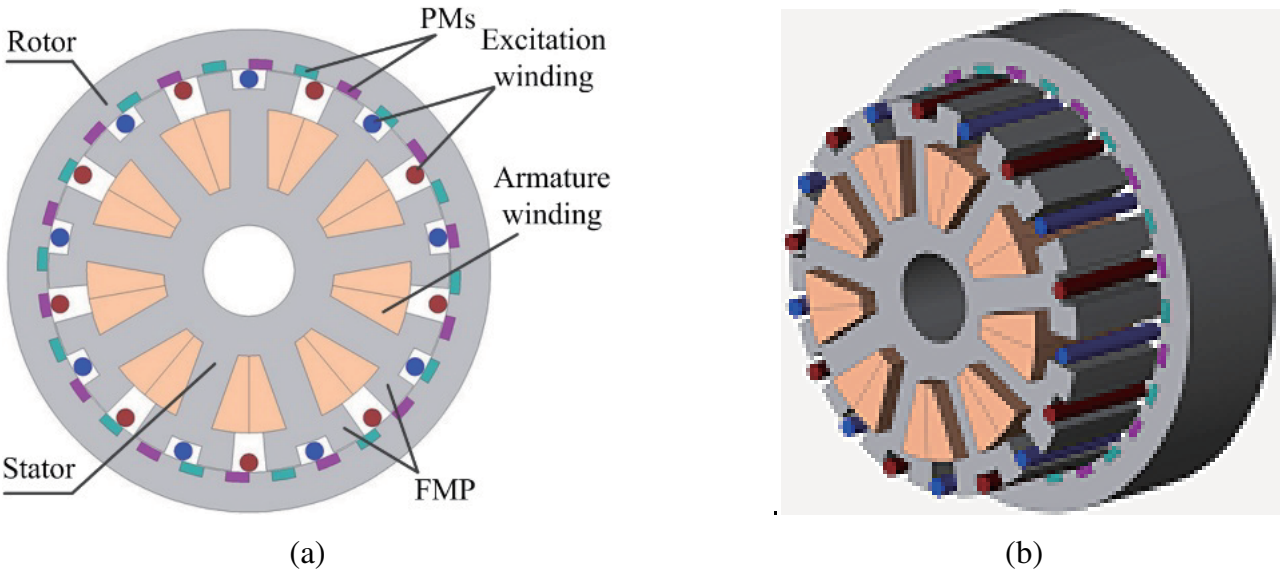

Figure 1. Proposed VFMFMM. (a) Machine configuration and (b) exploded view.

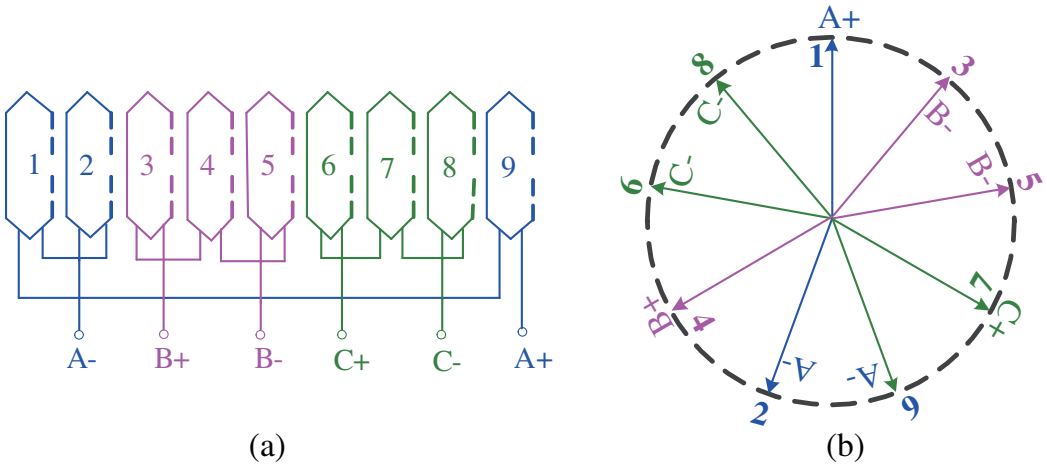

Figure 2. Proposed VFMFMM winding connection. (a) Stator armature winding connection, (b) stator armature winding connection star slot diagram.

magnetic field modulation principle of the magnetic field modulation motor and the advantages of low speed and high torque capacity. (2) However, the magnetic field distribution for the traditional PMVM is uncontrollable due to the single PM exaction, and it is not suitable to conduct wide speed regulation applications. The hybrid excitation is introduced into the field modulated motor, and the magnetic flux of the motor is adjustable by controlling the DC excitation winding [24]. (3) without increasing the complexity of the machine structure, the shortcoming for tractional PMVM is remedied by introducing additional DC excitation winding between adjacent FMPs, which can fulfill wide speed regulation range operation while exhibiting low speed and large torque merits. (4) The external rotor topology design is conducive to the design of vernier machine with multiple permanent magnets and can be directly combined with the electric vehicle hub. The rotor permanent magnet part adopts the alternate pole design to solve the problem of excessive use of permanent magnets in existing MFMMs. It can save the use of PMs and increase the mechanical strength of the rotor permanent magnet part.

3. PRINCIPLE ANALYSIS OF PROPOSED VFMFMM AND ITS TORQUE EXPRESSION

The proposed VFMFMM adopts armature and DC windings into the inner stator and FPMs, which means that the magnetic field distribution generated by the stator armature winding can be changed by the additional DC windings. At this time, the PMs can be considered as the tooth in the tractional magnetic gear, that is, a small position change on the rotor can lead to a large magnetic flux change for the whole machine. Based on the specific rules of the combination of pole and slot, the magnetic field of the stator armature winding with low pole pairs is modulated, thus, the harmonic magnetic field component that can match and interact with the high pole number PM magnetic field can be obtained. It means that the goal of low speed and high torque without increasing the machine volume and slot number can be obtained

$$P_{fw} = T_{\mathrm{FMP}_s} - P_r \tag{1}$$

where P_{fw} is the armature winding pole-pair in the stator; T_{FMPs} is the total number of FMPs; and P_r is the PM pole-pair.

Consequently, the high-to-low speed gear ratio of the proposed machine is given by [8]:

$$G_r = \frac{|iP_{fw} + jT_{\mathrm{FMP}_s}|}{iP_{vw}} \tag{2}$$

where $i = 1, 3, 5, \ldots$, and $j = 0, \pm1, \pm2, \ldots$, and when $i = 1$, $j = -1$, the largest modulation space harmonic component could be generated.

For the proposed machine, there are nine stator teeth. Two FMPs are uniformly distributed on each stator tooth, and eighteen FPMs are uniformly distributed on the whole stator. According to the magnetic gear modulation principle, the transmission ratio is 4.5. When the outer rotor speed is 200 rpm, the space rotating magnetic field speed of the stator armature winding is 900 rpm, which means that the outer rotor speed is only 1/4.5 of the space rotating magnetic field speed of the inner stator armature, which can achieve the magnetic field growth effect. That is, a small movement of the rotor makes a large change of the flux, which is called "magnetic gearing effect."

Electromagnetic torque of the proposed VFMFMM T_e consists of three parts, namely, the PM torque component T_{pm} generated by the action of PM flux linkage and armature winding current, the reluctance torque component T_r generated by the change of winding inductance, and the torque component T_f generated by the action of DC excitation winding flux linkage and armature winding [25], which is shown as

$$T_e = T_{pm} + T_r + T_f \tag{3}$$

When VFMFMM works at low-speed area, the reluctance torque is used as a part of the electromagnetic torque to increase the output torque, and no excitation current is applied. It can realize the direct drive operation at low speed and large torque through the magnetic flux modulation. When it works at the high-speed area, the DC excitation winding is energized, and the air gap magnetic density of the machine can be effectively suppressed to achieve high-speed field weakening control operation.

4. MODELING AND ANALYSIS OF VFMFMM ELECTROMAGNETIC CHARACTERISTIC

For the proposed VFMFMM, its remarkable feature is that there are two kinds of windings at the same time, so its working principle is different from that of traditional PMSM. Considering its unique topology and the working principle of flux modulation, the finite element method is used to calculate and analyze it.

$$\Omega : \frac{\partial}{\partial x}\left(\upsilon\frac{\partial A}{\partial x}\right) + \frac{\partial}{\partial y}\left(\upsilon\frac{\partial A}{\partial y}\right) = \sigma\frac{\partial A}{\partial t} - J - \upsilon\left(\frac{\partial B_{ry}}{\partial x} - \frac{\partial B_{rx}}{\partial y}\right) \tag{4}$$

where Ω is the field solution area, A the magnetic vector potential component, J the electric density, σ the conductivity, and B_{rx} and B_{ry} are remanence density, respectively.

The armature current in the proposed machine meets the following condition

$$\mu = L_e \frac{di}{dt} + Ri + \iint_{\Omega} \frac{\partial A}{\partial t} d\Omega \tag{5}$$

where u is the applied voltage, R the winding resistance, L_e the winding end inductance, l the axial length, S the area of any turn of wire in each phase winding, and Ω the total cross-sectional area of each phase winding.

The motion equation of the proposed machine is given as

$$T_e = J_m \frac{d\omega}{dt} + T_L + \lambda\omega \tag{6}$$

where J_m is the inertia of motion, ω the mechanical angular speed, T_L the load torque, and λ the damping coefficient.

The finite element model of the proposed motor can be obtained by combining Maxwell equations of Eq. (4) to Eq. (6).

The main specifications of the proposed VFMFMM are shown in Table 1.

When no current passes through the machine excitation winding, that is, when it is under no excitation, no-load magnetic field distributions of the proposed VFMFMM under different rotor positions are shown in Fig. 3.

It can be seen from Fig. 3 that although the field modulated motor is a branch of PMSM, its spatial magnetic field distribution is quite different from the traditional PMSM. The pole pairs of the stator windings of the traditional PMSM spatial magnetic field are equal to the pole pairs of the permanent magnet, while the pole pairs of the stator windings of the PMVM are no longer equal to the pole pairs of the permanent magnet. For the proposed VFPMVM, the permanent magnet pole pair is 14, and the stator winding space pole pair is 4. The flux is due to the PM, and between Figs. 3(a) and (b), there is a slight difference of the rotor positions, which corresponds to a quarter of the stator tooth pitch. It is noted that the number of pole pairs of the proposed VFPMVM flux distribution equals the value of P_{fw}. Thus, a steady torque is yielded by synchronizing the coil magnetomotive force (MMF) to the flux rotation. It is also observable that the flux distribution changes twenty electrical degrees with the indicated difference of the rotor position. That is, a small movement of the rotor makes a large change of the flux, which results in a high torque.

Figure 4 shows the no-load magnetic linkage and back-EMF waveform of the non excitation winding. The magnetic linkage and back-EMF waveform of the VFMFMM have a high sinusoidal degree, which is suitable for brushless AC drive, and its conduction angle is 180 degrees.

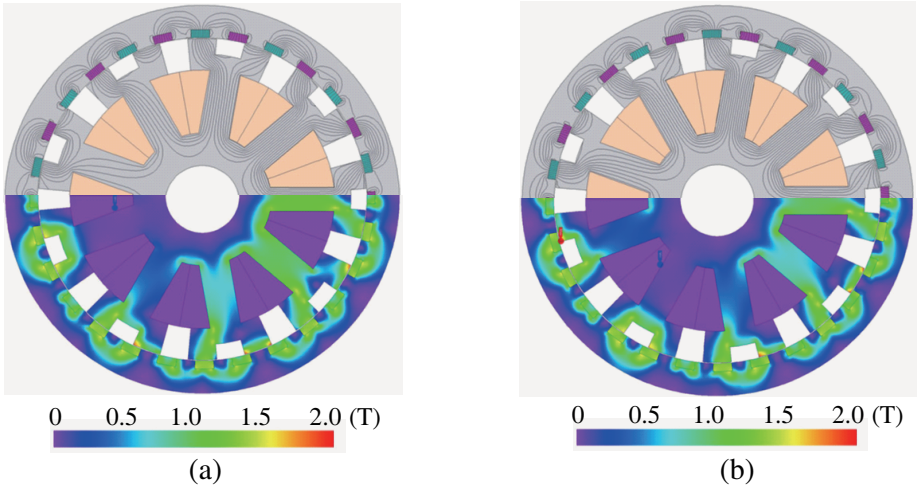

Figure 3. No-load magnetic field distributions with no excitation current. (a) Initial position, (b) twenty-degree movement.

Table 1. Main specifications of the proposed VFMFMM.

Item (symbol)	Value	Unit
Rated power: P_N	1000	W
Rated torque: T_N	47.6	N · m
Rated speed: n	214	rpm
Stator slots: Ns	9	-
Slot	3	-
Rotor pole number: N_r	14	-
Total Flux modulating poles number: T_{FMPs}	18	-
Gear ratio	4.5	-
Copper space factor	0.55	-
Rotor outer diameter	210	mm
Rotor inside diameter	180	mm
Stator outer diameter	179	mm
Stator inner diameter	24	mm
Air-gap length	0.5	mm
Stack length	60	mm
PM material type	Nd-Fe-B	-
PM remanence: B_r	1.3	T
PM width	13	deg

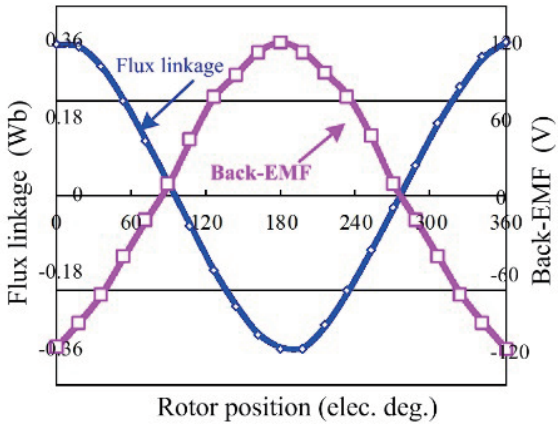

Figure 4. No-load flux linkage and back-EMF waveforms of the proposed VFMFMM.

According to the torque characteristic analysis and calculation expression of Eq. (14) in [6], for vernier machines, the harmonic coupling increases the machine torque when $Z_2 = Z_1 - p$ and decreases it when $Z_2 = Z_1 + p$, where Z_2, Z_1, and p are the numbers of stator teeth, rotor pole pairs, and winding pole pairs, respectively. For the proposed VFPMVM, the combination of P_{fw}, T_{FMPs}, and P_r replaces the Z_2, Z_1 and p, where P_{fw} is the number of armature winding pole-pairs in the stator, T_{FMPs} the total number of FMPs, and P_r the PM pole-pair. VFPMVM makes use of the air-gap fundamental and effective harmonic fields together to transmit the torque with unique flux modulation effect, which should be noticed that the fundamental spectrum is not equal to the number of PM pole-pairs. It can be seen from Fig. 6 that except for the 14^{th} fundamental component in the air gap flux space harmonics, the 4^{th} harmonic component in the high-speed low harmonic has the largest amplitude. Hence, the

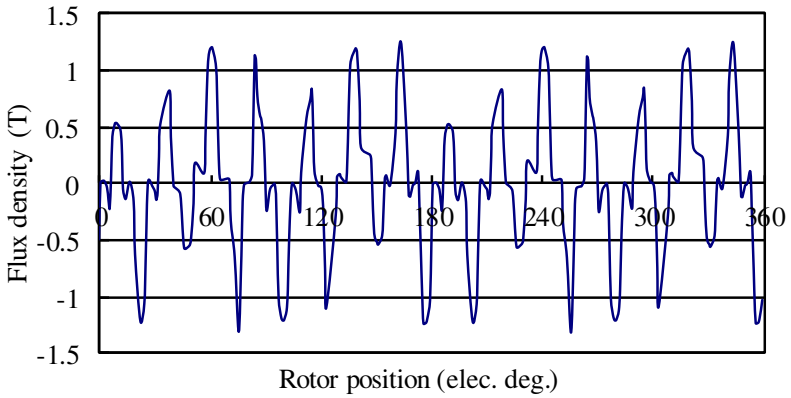

Figure 5. No-load radial air-gap flux density distribution.

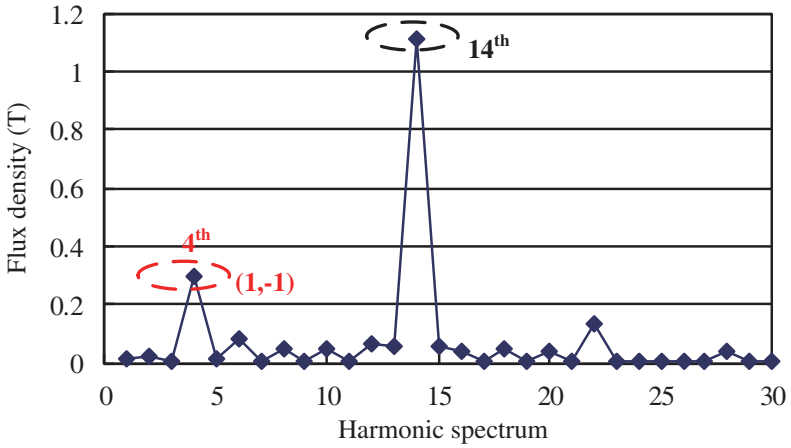

Figure 6. No-load radial air-gap flux density harmonic spectrum.

combination of the 4^{th} and 14^{th} harmonic components yields the largest output torque. The radial flux density distribution of the machine is shown in Fig. 5. There are 14 air-gap magnetic density cycles in 360 degrees, which verifies the design of 14 pairs of PMs of the machine. The corresponding harmonic spectrum is shown in Fig. 6. It can be seen from Fig. 6 that except for the 14^{th} fundamental component in the air gap flux space harmonics, the 4^{th} harmonic component in the high-speed low harmonic has the largest amplitude. The 4^{th} harmonic corresponds to the transmission ratio of 4.5, as an effective harmonic component, which is part of the output torque. It verifies the principle of magnetic flux modulation. In addition, it can be seen from Fig. 6 that the peak value of air-gap flux density of the proposed VFPMVM is higher than that of the traditional alternating pole PMSM, which verifies that the flux modulation effect is helpful for improving the machine output torque, so as to increase the torque density.

The steady state output torque and cogging torque characteristics of VFPMVM are shown in Fig. 7. It can be seen from the figures that the designed machine has a high output torque; the average torque reaches 47.5 Nm; and the torque density is higher than the variable flux vernier machine proposed in the literature. In addition, the cogging torque of the machine is 0.98 Nm, which is only 1.9% of the steady state torque.

Moreover, with the purpose of investigating the relationship between the FMP number and the cogging torque, the variations of the cogging torque with different stator auxiliary teeth N_{FMP} are shown in Fig. 8. The values of N_{FMP} are 0 and 1, which means the stator single tooth and multi-tooth structure, respectively. The peak values of the cogging torque are 1.22 Nm and 0.98 Nm when N_{FMP} is

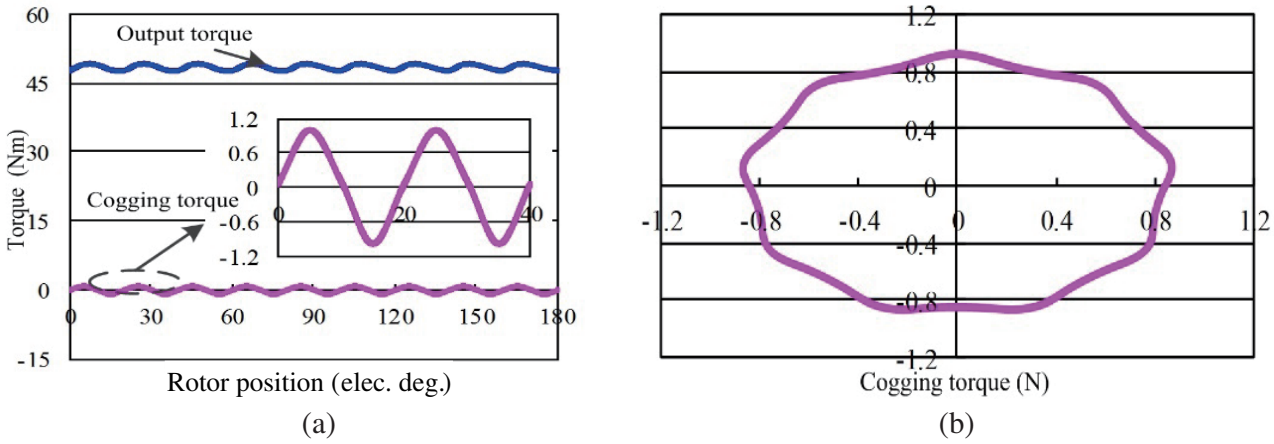

Figure 7. VFPMVM torque characteristics. (a) Output torque, (b) cogging torque.

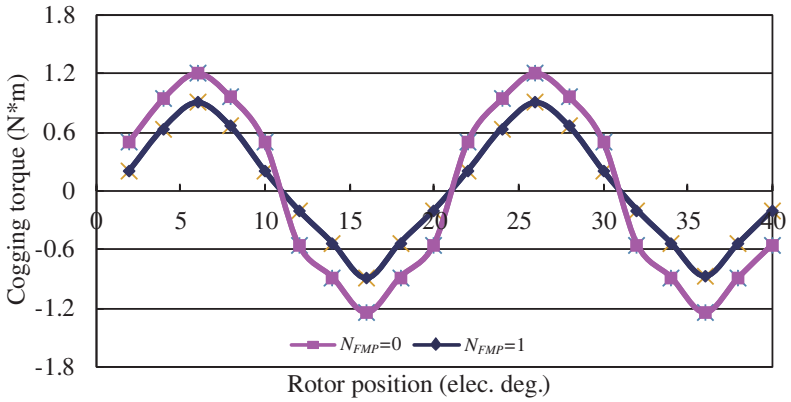

Figure 8. The cogging torque comparisons with different N_{FMP}.

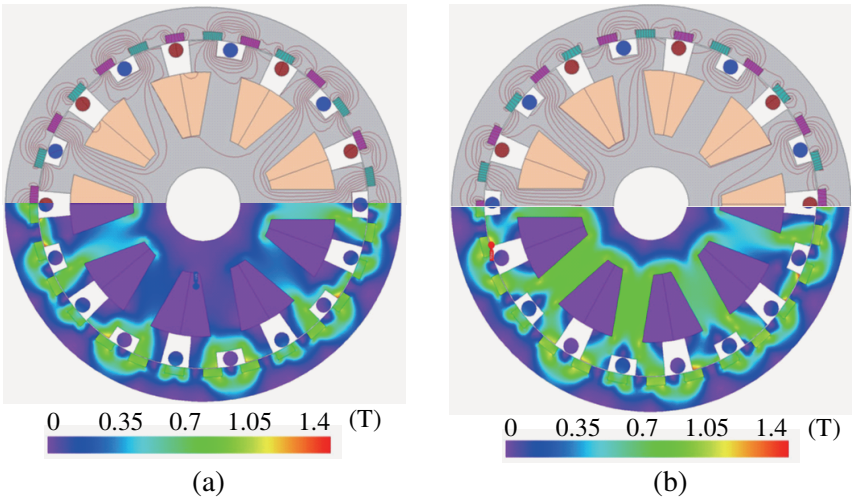

Figure 9. VFPMVM magnetic flux distribution with excitation current. (a) Initial position, (b) twenty-degree movement.

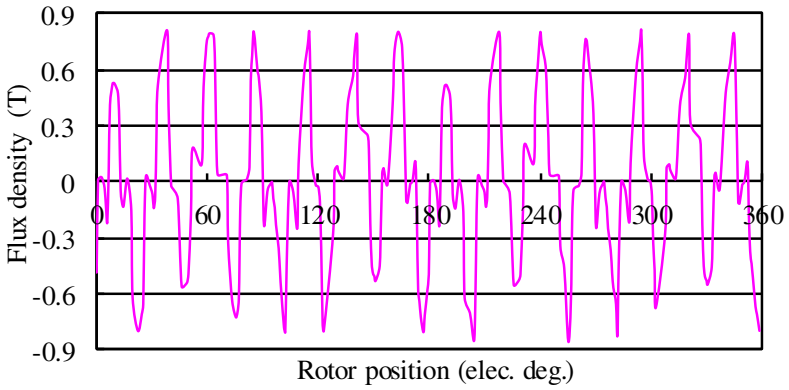

Figure 10. VFPMVM air-gap flux density distribution with excitation current.

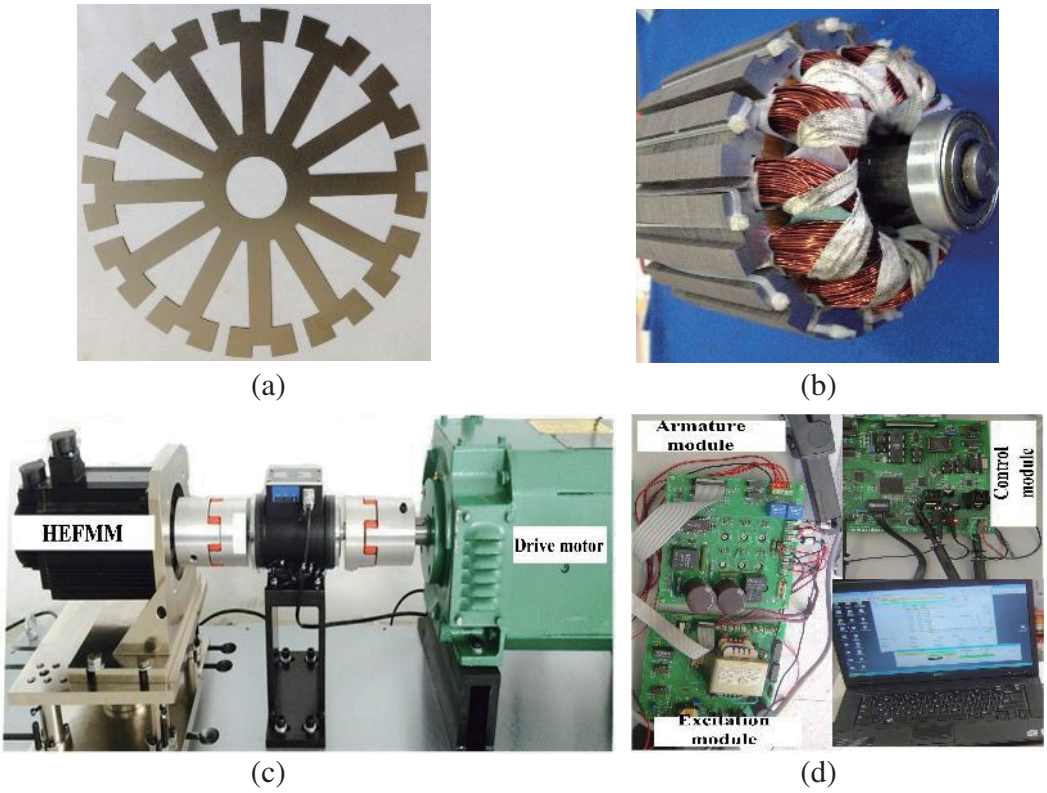

Figure 11. VFPMVM test system with (a) prototype stator lamination, (b) prototype stator with armature winding, (c) prototype test platform and (d) control system.

equal to 0 and 1, respectively in Fig. 8., namely, the cogging torque is reduced by 19.6% compared with that without the auxiliary slot. It means that the multi-tooth fractional slot structure is beneficial to reducing cogging torque for the proposed machine. The fact that the peak value of the cogging torque when $N_{\mathrm{FMP}} = 1$ is minimum is because the influence by low order harmonics is greatly weakened.

When the excitation current is applied, the magnetic field line and magnetic density distribution of the VFMFMM are shown in Fig. 8. It can be seen from Fig. 9 that the magnetic density distribution is greatly affected after the excitation current is applied to the machine.

After the excitation current is applied, the distribution of VFPMVM air gap magnetic density is shown in Fig. 10. Compared with Fig. 5, the air gap magnetic density of the machine is significantly

reduced compared with that without the excitation winding, which proves the effectiveness of magnetic field weakening control.

5. EXPERIMENTAL VERIFICATIONS

With the purpose of verifying the correctness of simulations results with the proposed VFMFMM, a 1 kW prototype and its testing platform were established, as shown in Fig. 11.

Figure 12 shows the test waveforms of back-EMF when the excitation currents are 0, 0.5 A, −0.5 A, and machine operation speeds are 100 rpm, 150 rpm, and 200 rpm, respectively. It can be seen from Fig. 11 that the back-EMF values change obviously when the excitation current values are changed. When the excitation current values are 0.5 A and −0.5 A, the average field weakening and increasing amplitudes are 52.9% and 33.7%, respectively, which can meet the needs of wide speed range regulation. It is worth noting that, compared with the traditional hybrid excitation PMSM, the proposed VFMFMM in this paper has more obvious effect in the field weakening, and the magnetic field saturation of the machine is easier to be obtained caused by the increase of magnetic field.

Figure 13 shows the back-EMF waveform of the proposed machine at the rated speed of 214 rpm without DC excitation. It can be seen from the figure that the three-phase back-EMF waveforms are symmetrical in phase, and the waveforms are sinusoidal. The effective value of the fundamental wave of the VFMFMM back-EMF is 88.6 V, and its total harmonic distortion (THD) rate is 1.56%.

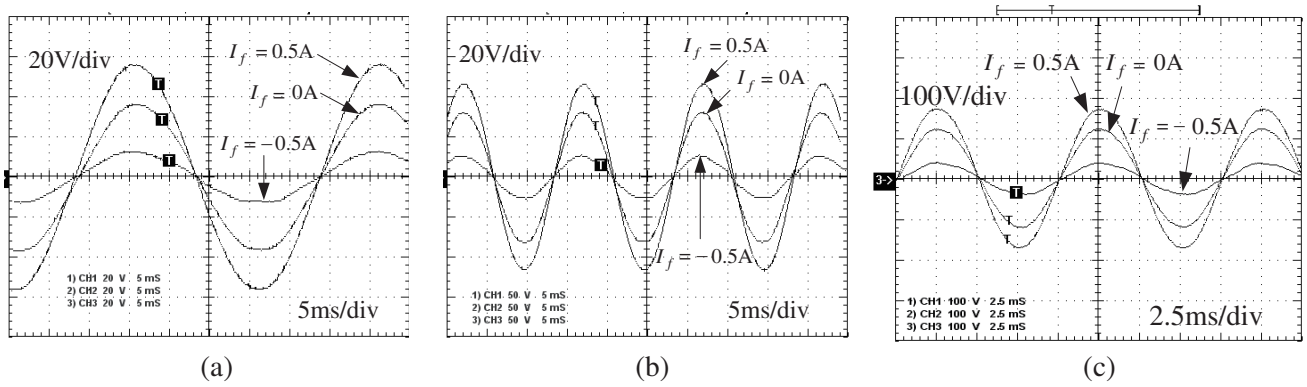

Figure 12. Different back-EMF waveforms with excitation current values of I_f are 0, 0.5 A and −0.5 A. (a) $n = 100$ rpm, (b) $n = 150$ rpm, (c) $n = 200$ rpm.

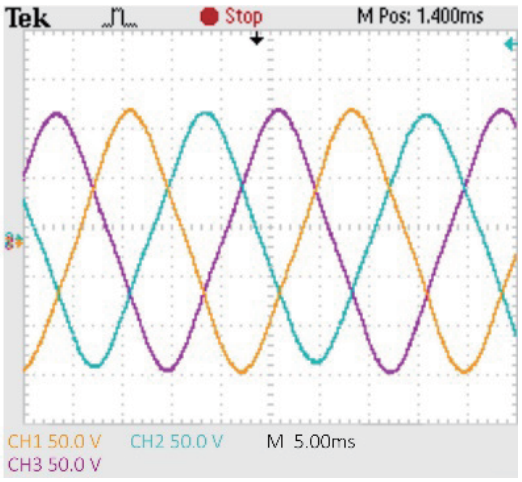

Figure 13. Back-EMF waveform with no excitation current at rated speed.

6. CONCLUSION

Based on introducing hybrid excitation principle into the magnetic field modulation machine, a new type of VFMFMM is presented and designed in this paper. Based on the magnetic field modulation, the VFMFMM mathematical model was deduced, and its FEA model was established. According to the magnetic field adjusting property of VFMFMM, one DC excitation control method for VFMFMM was presented. The operating performance of the machine was investigated in the entire operating region. Both simulated and experimental results verify the validity of the proposed machine performance, and the following conclusions could be drawn:

(1) The stator adopts a multi-tooth split pole structure, which can effectively reduce the number of stator slots and provide more space to accommodate the armature winding. The operation range of the proposed machine is enlarged without increasing the machine volume and the number of stator slots.

(2) By separating the DC excitation winding from the stator slot, the utilization of stator space can be effectively improved, thus effectively improving the motor torque density.

(3) The concentrated winding structure can effectively shorten the armature winding end and reduce the motor loss, while the multi-pole fractional slot helps to reduce the motor cogging torque.

(4) One prototype with 1 kW rated power is designed, and the corresponding characteristics are tested. The experimental results show that the proposed machine has high torque output at low speed, small cogging torque, and good dynamic field weakening speed regulation capacity, which has a good application prospect in the field of low-speed direct drive for EVs.

ACKNOWLEDGMENT

This work was supported by Scientific and Technological Program of Henan Science and Technology Agency (212102210022, 212102210014), the Natural Science Foundation of Henan Province (212300410127), the Scientific Research and Cultivation Foundation of Henan University of Engineering, and the National Natural Science Foundation of P. R. China (62173126).

REFERENCES

1. Chan C. C, K. T. Chau, and J. Z. Jiang, "Novel permanent magnet motor drives for electric vehicles," *IEEE Trans Ind Electr.*, Vol. 43, No. 2, 331–339, 1996.
2. Chan C. C., "The state of the art of electric, hybrid, and fuel cell vehicles," *Proc. of the IEEE*, Vol. 95, No. 4, 704–718, 2007.
3. Zhu, Z. Q. and D. Evans, "Overview of recent advances in innovative electrical machines-with reference to magnetically geared switched flux machines," *Proceedings of International Conference on Electrical Machines and Systems*, 1–10, 2014.
4. Amara, Y., J. Lucidarme, M. Gabsi, M. Lécrivain, A. Hamid, B. Ahmed, and A. D. Akémakou, "A new topology of hybrid synchronous machine," *IEEE Trans. Ind. Appl.*, Vol. 37, No. 5, 1273–1278, 2001.
5. Wang, L. L., J. X. Shen, P. C. K. Luk, W. Z. Fei, C. F. Wang, and H. Hao, "Development of a magnetic-geared permanent-magnet brushless motor," *IEEE Trans. Magn.*, Vol. 45, No. 10, 4578–4581, 2001.
6. Toba, A. and T. A. Lipo, "Generic torque-maximizing design methodology of the surface permanent magnet vernier machine," *IEEE Trans. Ind. Appl.*, Vol. 36, No. 6, 1539–1546, 2000.
7. Chau, K. T., D. Zhang, J. Z. Jiang, C. Liu, and Y. Zhang, "Design of a magnetic-geared outer-rotor permanent-magnetic brushless motor for electric vehicles," *IEEE Trans. Magn.*, Vol. 43, No. 6, 2504–2506, 2007.
8. Jian, L. N. and K. T. Chau, "Analytical calculation of magnetic field distribution in coaxial magnetic gears," *Progress In Electromagnetics Research*, Vol. 92, 1–16, 2009.
9. Jian, L. N. and K. T. Chau, "Design and analysis of a magnetic-geared electronic-continuously variable transmission system using finite element method," *Progress In Electromagnetics Research*, Vol. 107, 47–61, 2010.

10. Jian, L. N., G. Xu, Y. Gong, J. Song, J. Liang, and M. Chang, "Electromagnetic design and analysis of a novel magnetic-gear-integrated wind power generator using time-stepping finite element method," *Progress In Electromagnetics Research*, Vol. 113, 351–367, 2011.
11. Jian, L. N., G. Xu, J. Song, H. Xue, and D. Zhao, "Optimum design for improving modulating-effect of coaxial magnetic gear using response surface methodology and genetic algorithm," *Progress In Electromagnetics Research*, Vol. 116, 297–312, 2011.
12. Xu, G., L. N. Jian, W. Gong, and W. Zhao, "Quantitative comparison of flux-modulated interior permanent magnet machines with distributed windings and concentrated windings," *Progress In Electromagnetics Research*, Vol. 129, 109–123, 2012.
13. Li, J. G., K. T. Chau, J. Z. Jiang, C. H. Liu, and W. Li, "A new efficient permanent-magnet vernier machine for wind power generation," *IEEE Trans. Magn.*, Vol. 46, No. 6, 1475–1478, 2010.
14. Jian, L. N., J. N. Liang, Y. J. Shi, and G. Xu, "A novel double-winding permanent magnet flux modulated machine for stand-alone wind power generation," *Progress In Electromagnetics Research*, Vol. 142, 275–289, 2013.
15. Kong W. Q., Y. Zhang, M. M. Huang, and Q. Z. Huang, "Flux concentrating multi-tooth splitting poles permanent magnet vernier machine cogging torque optimization and experimental verification," *INT J. Appl. Electrom*, Vol. 56, No. 4, 1–12, 2018.
16. Xu, L., W. X. Zhao, G. H. Liu, and C. Song, "Design optimization of a spoke-type permanent-magnet vernier machine for torque density and power factor improvement," *IEEE Trans. Veh. Technol.*, Vol. 68, No. 4, 3446–3456, 2019.
17. Zhang, Y., D. Li, P. Yan, X. Ren, and J. Ma, "A high torque density claw pole permanent-magnets vernier machine," *IEEE Trans. Ind. Electron.*, Vol. 10, No. 2, 1756–1765, 2022.
18. Guan, Q., Y. T. Fang, and P. D. Pfister, "A novel concentrated-winding vernier pseudo-direct-drive permanent-magnet machine," *IEEE Trans. Magn.*, Vol. 58, No. 2, 8103805, 2022.
19. Wu, L. L. and R. H. Qu, "A novel dual-stator vernier permanent magnet machine with improved power factor," *IEEE Trans. Ind. Appl.*, Vol. 58, No. 3, 3486–3496, 2022.
20. Li, X. L., K. T. Chau, and M. Cheng, "Analysis, design and experimental verification of a field-modulated permanent-magnet machine for direct-drive wind turbines," *IET Electr. Power Appl.*, Vol. 9, No. 2, 150–159, 2015.
21. Yang, H., H. Y. Lin, Z. Q. Zhu, S. H. Fang, and Y. K. Huang, "Novel flux-regulatable dual-magnet vernier memory machines for electric vehicle propulsion," *IEEE Trans. Appl. Supercond.*, Vol. 24, No. 5, 0601205, 2014.
22. Zhang, Y., H. Y. Lin, S. H. Fang, and Y. K. Huang, "Comparison and analysis of dual stator permanent magnet vernier machines with different pole/slot combinations for low speed direct drive applications," *Int J. Appl. Electrom.*, Vol. 50, 617–626, 2016.
23. Liu, C. H., J. Zhong, and K. T. Chau, "A novel flux-controllable vernier permanent-magnet machine," *IEEE Trans. Magn.*, Vol. 47, No. 10, 4238–4241, 2011.
24. Amara, Y., L. Vido, M. Gabsi, E. Hoang, and B. Hamid, "Hybrid excitation synchronous machines: Energy-efficient solution for vehicles propulsion," *IEEE Trans. Veh. Technol.*, Vol. 58, No. 5, 2137–2149, 2009.
25. Zhang, Y., Q. Z. Huang, and M. M. Huang, "Design and experimental verification of adaptive speed region control for hybrid excitation claw-pole synchronous machine," *Progress In Electromagnetics Research C*, Vol. 88, 195–205, 2018.